Transcriptome transfer produces a predictable cellular phenotype

Jai-Yoon Sul[a,1], Chia-wen K. Wu[a,1], Fanyi Zeng[a,b,1], Jeanine Jochems[a], Miler T. Lee[c,d], Tae Kyung Kim[a], Tiina Peritz[a], Peter Buckley[a,c], David J. Cappelleri[e], Margaret Maronski[f], Minsun Kim[g], Vijay Kumar[c,e], David Meaney[c,h], Junhyong Kim[c,d,1], and James Eberwine[a,c,i,1,2]

Departments of [a]Pharmacology, [c]Penn Genome Frontiers Institute, [d]Biology, [e]Mechanical Engineering and Applied Mechanics, [f]Neuroscience, [h]Bioengineering, and [i]Psychiatry, University of Pennsylvania, Philadelphia, PA 19104; [b]Shanghai Institute of Medical Genetics and Institute of Medical Sciences, Shanghai Jiao Tong University School of Medicine, Shanghai 200040, Peoples Republic of China; and [g]Department of Physiology, Wonkwang University School of Medicine, Iksan 570-749, South Korea

Communicated by William T. Greenough, University of Illinois, Urbana, IL, March 5, 2009 (received for review January 23, 2009)

Cellular phenotype is the conglomerate of multiple cellular processes involving gene and protein expression that result in the elaboration of a cell's particular morphology and function. It has been thought that differentiated postmitotic cells have their genomes hard wired, with little ability for phenotypic plasticity. Here we show that transfer of the transcriptome from differentiated rat astrocytes into a nondividing differentiated rat neuron resulted in the conversion of the neuron into a functional astrocyte-like cell in a time-dependent manner. This single-cell study permits high resolution of molecular and functional components that underlie phenotype identity. The RNA population from astrocytes contains RNAs in the appropriate relative abundances that give rise to regulatory RNAs and translated proteins that enable astrocyte identity. When transferred into the postmitotic neuron, the astrocyte RNA population converts 44% of the neuronal host cells into the destination astrocyte-like phenotype. In support of this observation, quantitative measures of cellular morphology, single-cell PCR, single-cell microarray, and single-cell functional analyses have been performed. The host-cell phenotypic changes develop over many weeks and are persistent. We call this process of RNA-induced phenotype changes, transcriptome-induced phenotype remodeling.

neuron | transcriptome-induced phenotype remodeling | single cell | Waddington

In multicellular organisms, all cells contain nearly identical copies of the genome but exhibit drastically different phenotypes. Even a single neuron has a set of phenotypic characteristics that distinguish it from other neurons as well as other cell types, such as the nearby astrocytes. Indeed, as Waddington proposed in his classical epigenetic landscape model, genetically predetermined cells can follow any specific permitted trajectories that eventually lead to different cellular phenotypes (1). From this point of view, the genome serves as a repository of dynamic control information whose state can be reprogrammed to match the stable phenotypic states.

Emerging evidence has demonstrated the reversibility and flexibility of the cellular phenotype. Gurdon et al. first showed that the ability to obtain fertile adult male and female frogs by injecting endoderm nuclei into enucleated eggs (2). This result not only forms the foundation of the field in nuclear transplantation but also provides evidence that the cytoplasmic components of a differentiated cell can support nuclear reprograming. Generation of induced pluripotent stem (iPS) cells by transfection of transcription factors into dividing fibroblasts (3), followed by cell selection, represents a new strategy to globally revert a mature cell into a different cell type (4–9). The need for redifferentiation of these embryonic stem cell-like-iPS cells into desired cell types adds a layer of complexity that is difficult to control (10, 11). Nevertheless, studies of nuclear reprogramming from genomic and epigenetic modification, as seen from somatic-cell nuclear-transfer-cloned animals and iPS cells, strongly demonstrate the flexibility of a differentiated phenotype, as well as the dynamic changes of a genome (7). A key question is whether there is a general strategy to efficiently reprogram a cell to any target-cell type.

cDNA microarray analysis has shown that phenotypic differences at the cellular level are associated with differences in the presence, absence, and abundance of particular RNAs. As the transcriptome contains the RNAs that encode the proteins necessary to generate and maintain phenotype, such as kinases, phosphatase, histone acetylases and deacetylases, and other proteins, including transcription factors that collaborate in the right proportions to generate the phenotype, it is reasonable to assume it has a dominant role in determining phenotype. To test this hypothesis using single-cell approaches, we introduced the transcriptome from donor cells into individual host cells and quantitatively assessed conversion from the host to the donor cell phenotype (12, 13).

Results

Modeling of the Phototransfection of Complex RNA Populations. To evaluate whether the astrocyte transcriptome can directly convert host neurons into astrocytes, we first characterized our cell cultures to ensure the purity of the neurons that are to be transfected [supporting information (SI) Fig. S1] and then established a working transcriptome-induced phenotype remodeling (TIPeR) protocol, which consists of multiple RNA phototransfections over a 10-day period (Fig. 1*A*). Phototransfection was selected as the means to transfect the astrocyte transcriptome into neurons, as it can transfect RNA into neurons with high efficiency (12). To optimize for the amount of RNA that can be introduced into the host cells, we modeled the phototransfection of RNA transcripts that diffuse into the photoinduced pores on the cell membranes (Fig. S2). This process was modeled with an average transcript size of 1.5 kb ± 0.2 kb with the effective radius of the transcript determined by the Flory approximation ($R_{transcript} \approx 5.5N^{1/3}$, where N is the size of the transcript in bases). Pore sizes were systematically varied to test the relative flux of transcriptome in a typical phototransfection experiment. Simulations with the approximated transcriptome cargo showed that a single sequence of 16 pulses across the cell membrane would be sufficient to deliver a large number of transcripts while retaining their relative abundances (Fig. 1 *B* and

Author contributions: J.-Y.S., C.K.W., F.Z., M.T.L., T.K.K., T.P., D.J.C., M.K., V.K., D.M., J.K., and J.E. designed research; J.-Y.S., C.K.W., F.Z., J.J., M.T.L., T.K.K., T.P., P.B., D.J.C., M.K., V.K., J.K., and J.E. performed research; J.-Y.S., M.T.L., D.J.C., M.M., V.K., D.M., J.K., and J.E. contributed new reagents/analytic tools; J.-Y.S., C.K.W., F.Z., J.J., M.T.L., T.K.K., T.P., P.B., D.J.C., M.K., V.K., D.M., J.K., and J.E. analyzed data; and J.-Y.S., C.K.W., F.Z., J.J., M.T.L., T.P., P.B., D.J.C., M.M., M.K., V.K., D.M., J.K., and J.E. wrote the paper.

Conflict of interest: William T. Greenough and J.E. have collaborated on past research. They are not currently collaborating. The remaining authors declare no conflict of interest.

Freely available online through the PNAS open access option.

[1]J.-Y. S, C.K.W., F.Z., J.K., and J.E. contributed equally to this work.

[2]To whom correspondence should be addressed. E-mail: eberwine@upenn.edu.

This article contains supporting information online at www.pnas.org/cgi/content/full/0902161106/DCSupplemental.

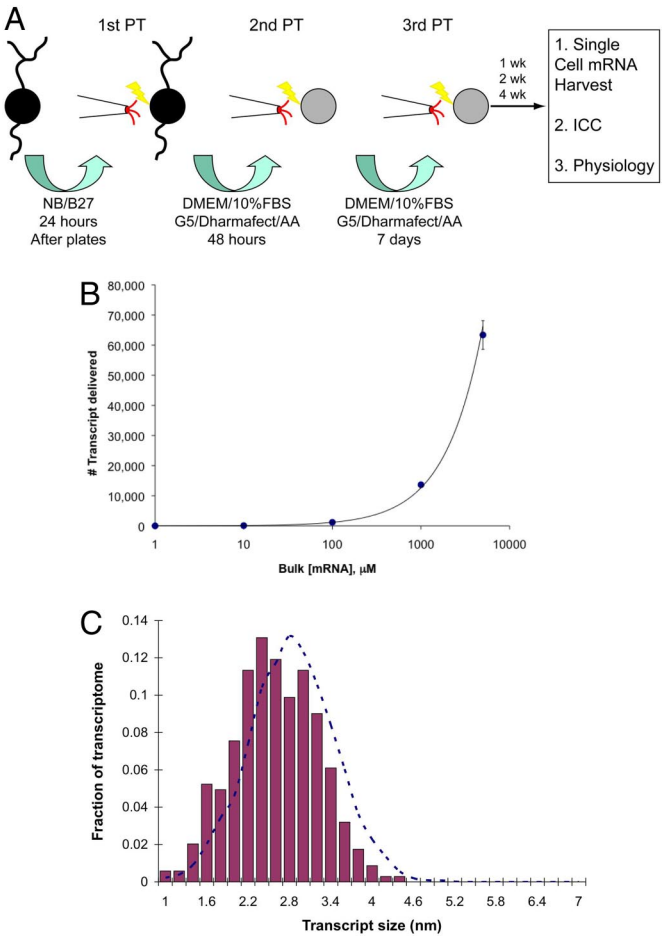

Fig. 1. Modeling of TIPeR process. (*A*) The first phototransfection was performed on hippocampal neurons with local delivery of the astrocyte transcriptome. The same procedure was repeated 48 h and 7 days after the first phototransfection. Single-cell mRNA harvesting, immunocytochemistry, and physiological assessment were performed at various times after the third phototransfection. (*B*) Given the ability to control transport of molecules across the plasma membrane through both the number of pulses and extracellular concentrations, simulations were conducted to estimate the efficacy of mRNA transfer through a standard phototransfection pulse. (*C*) The dashed line is the histogram showing the size distribution of the transcripts in solution during phototransfection. The bars show the amount of the transcript delivered into the cytosol. There is a slight reduction in delivery efficiency of the largest transcripts, as their sizes are on the order of the assumed size of the phototransfection pore. For a transcriptome that contained a large range of transcript sizes, simulations indicated that the relative composition of the delivered cargo to the cytosol would largely remain intact.

C). Based upon this simulation and empirical tests, we used a 200 ng/μl concentration of polyA+-selected RNA for the TIPeR experiments. This is estimated to result in ≈160,000 transcript molecules being delivered into the TIPeR cells in each phototransfection session, which is in excess of the normal contingent of mRNA transcripts of a hippocampal neuron (≈100,000 molecules).

Astrocyte mRNA TIPeRed Neurons Stably Express Donor-Specific Astrocytic Markers. We assessed the expression of the astrocytic marker GFAP and the neuronal marker microtubule-associated protein 2 (MAP2) in the neurons TIPeRed with the astrocyte transcriptome, which we designate N-TIPeR-AS to indicate that a neuron (N) was transfected with astrocyte (AS) RNA. We harvested the individual N-TIPeR-AS cells at 3 time points following the third phototransfection (see Fig. 1*A*, 1-, 2- and 4-weeks later), and then performed nested single-cell RT-PCR and sequence verification to assay GFAP and MAP2 mRNAs. Data in Fig. 2 show that 10 out of 26 N-TIPeR-AS cells across 4 weeks after the last phototransfection displayed GFAP gene expression. A subset of the GFAP-expressing N-TIPeR-AS cells (8 cells) also expressed the neuronal MAP2 mRNA, suggesting that these cells are intermediate between neuronal and astrocytic phenotypes. Finally, 2 cells showed no detectable *MAP2* gene expression in the RT-PCR assay, showing that *MAP2* gene expression has been turned off in these cells.

We next asked whether the N-TIPeR-AS cells also expressed astrocytic protein markers. We performed triple-labeled immunocytochemistry on the N-TIPeR-AS cells using antibodies against the neuronal marker NeuN and the astrocytic marker GFAP. Additionally, we used an antibody against the higher abundance astrocytic-marker fibronectin, which is the seventh-most abundant mRNA relative to GFAP, which is the 191st most-abundant mRNA as observed in single astrocyte microarray analysis. No fibronectin mRNA or protein is detected in neurons. Immunocytochemical analysis of NeuN, GFAP, and fibronectin in N-TIPeR-AS cells 2 weeks after the last phototransfection show that astrocytic markers GFAP and fibronectin coexpressed with the neuronal marker NeuN (see Fig. 2*B*). GFAP-protein expression is low, while fibronectin is more abundant in these cells. Similar to the RT-PCR results, the N-TIPeR-AS cells coexpressing all 3 antigens suggests that the 2-week N-TIPeR-AS cells are at an intermediate phenotypic state between neurons and astrocytes. We also performed a distinct set of immunocytochemistry studies with the neuronal specific anti-Dynamin 1 antibody and anti-GFAP. To assess the expression levels, we analyzed the integrated fluorescence signal strength of targeted cell area (see Fig. 2*C*). The results show that the expression patterns of Dynamin 1 and GFAP of TIPeR cells are similar to that of astrocytes, while neurons had a distinctive pattern.

N-TIPeR-AS Cells Display Global Alteration in Overall Gene Expression Profile. We assayed single-cell transcriptomes of neurons, astrocytes, control cells (neurons TIPeRed with neuron transcriptome, designated as N-TIPeR-N), and N-TIPeR-AS cells. RNA from 48 individual cells was each isolated, amplified, and assayed with Affymetrix Rat Genome 230 2.0 GeneChips. Fig. 3*A* shows a cluster diagram of the single-cell transcriptomes for a set of 3,104 informative genes and the bootstrap support of the clusters (see *Materials and Methods*). Out of 27 N-TIPeR-AS cells, 12 (44%) cells consistently clustered with the astrocytes 91% of the time, indicating expression profiles similar to the normal variation in astrocytes. We designate these 12 TIPeR cells as astro-TIPeRs, while the other 15 N-TIPeR-AS cells that do not cluster with the astrocytes are designated neuro-TIPeRs. Control cells (N-TIPeR-N) were distinct from astrocytes with only 3% of the bootstrap samples clustering control cells with astrocytes. Fig. 3*B* shows a 3-dimensional projection of the 3,104-gene transcriptome along 3 biologically meaningful directions: (*i*) genes differentiating astrocytes and neurons; (*ii*) genes showing large N-TIPeR-AS variation; and (*iii*) genes that are most variable in all cells (see *Materials and Methods*). This 3-dimensional plot shows how the transcriptome of individual cells delimit a variable but a distinct region of identity for each cell types (lightly shaded cloud around the composite cells). Any cell within this region of identity would be classified phenotypically as the same cell type. The N-TIPeR-AS cell transcriptomes were measured at 1 week, 2 weeks, and 4 weeks after the third phototransfection. Interestingly, 3 out of 9 of the 1-week cells, 4 out of 7 of the 2-week cells, and 5 out of 11 of the 4-week cells fell into the astro-TIPeR category, showing an increasing astrocytic conversion (30%–50%) between 1 and 2 weeks postphototransfection age (see Fig. 3*A*).

De Novo, Up- and Down-Regulation of Genes Are Seen in TIPeR Cells. To dissect the genes that differentiate successful TIPeR cells, we carried out paired comparisons between astro-TIPeR cells, neurons, and astrocytes (*SI Materials and Methods*). A total of 532 genes

A

Cell Name	Age (week)	Primer sets GFAP	MAP2
1A	1		
1B	1		+
1C	1		+
1D	1		+
1E	1		+
1F	1		+
1G	1	+	+
1H	1	+	+
2A	2		
2B	2		+
2C	2		+
2D	2		+
2E	2		+
2F	2	+	+
2G	2	+	+
2H	2	+	
2I	2	+	
4A	4		
4B	4		+
4C	4		+
4D	4		+
4E	4		+
4F	4	+	+
4G	4	+	+
4H	4	+	+
4I	4	+	+
Population cortex cells		+	+
No template			

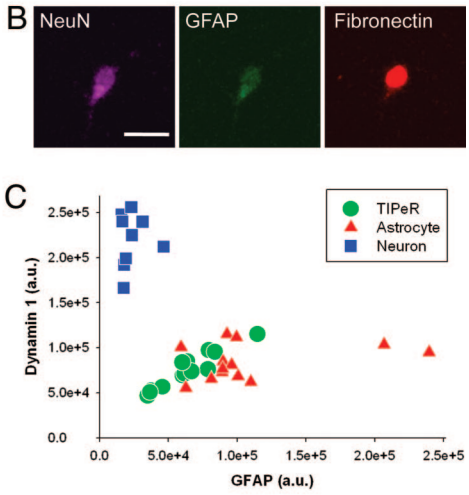

Fig. 2. N-TIPeR-AS cells coexpressed astrocytic and neuronal mRNA and protein markers. (*A*) Single-cell RT-PCR was performed on N-TIPeR-AS cells at different time points to detect the expression of *GFAP* and *MAP2* genes. Age was defined as time after the third phototransfection. "+" indicates the presence of GFAP or MAP2 mRNA., GFAP-positive cells are highlighted with shadows. Population brain-cortex cells containing both neurons and astrocytes were used as positive control and water was the negative control. (*B*) The representative N-TIPeR-AS cell is immunoreactive for all NeuN, GFAP, and fibronectin antibodies 2 weeks after the third phototransfection. (Scale bar, 10 μm.) (*C*) The table shows the immunoreactivity of Dynamin 1 and GFAP in the astrocyte (*red triangle*), the neuron (*blue square*), and the TIPeR cell (*green circle*). The graph shows that integrated immunofluorescence signal from regions of interest. The TIPeR cells are clustered with the astrocytes and are distinct from the neuron cluster.

significantly distinguish neurons from astrocytes with at least 2-fold intensity difference. These genes separated into 4 sets: (A) TIPeR expression equals astrocytes does not equal neurons, (B) TIPeR expression equals neurons does not equal astrocytes, (C) intermediate TIPeR expression, and (D) TIPeR expression different from both neurons and astrocytes (see Fig. 3*C*). A geneontology (GO) enrichment analysis was carried out to assess the functional significance of the 4 groups (see Table S1). The up-regulated genes in group (A) show greatest enrichment in the transcriptional activity category (RNA Pol II activity, RNA metabolic process, nucleic acid binding, gene expression), while the down-regulated genes were most enriched in the cell division and cytokinesis categories, as well as transmembrane transporter activity. It should be noted that down-regulated cell-division genes does not mean that cell division itself is inhibited in successful TIPeR cells (compare p53's activity in cell proliferation). Group (B) genes represent genes that have failed to move toward astrocytes. These genes are enriched for glutamine metabolic process, spindle pole, and chromosomes (up-regulated), as well as antioxidant pathways (down-regulated). Of the genes whose TIPeR expression is neither astrocyte-like nor neuron-like (group C), notable enrichment of intracellular membrane-bound organelle-related processes were found.

Because the half-life of GFAP mRNA is 4 h (14), the *GFAP* gene expression in N-TIPeR-AS cells at 4 weeks after phototransfection

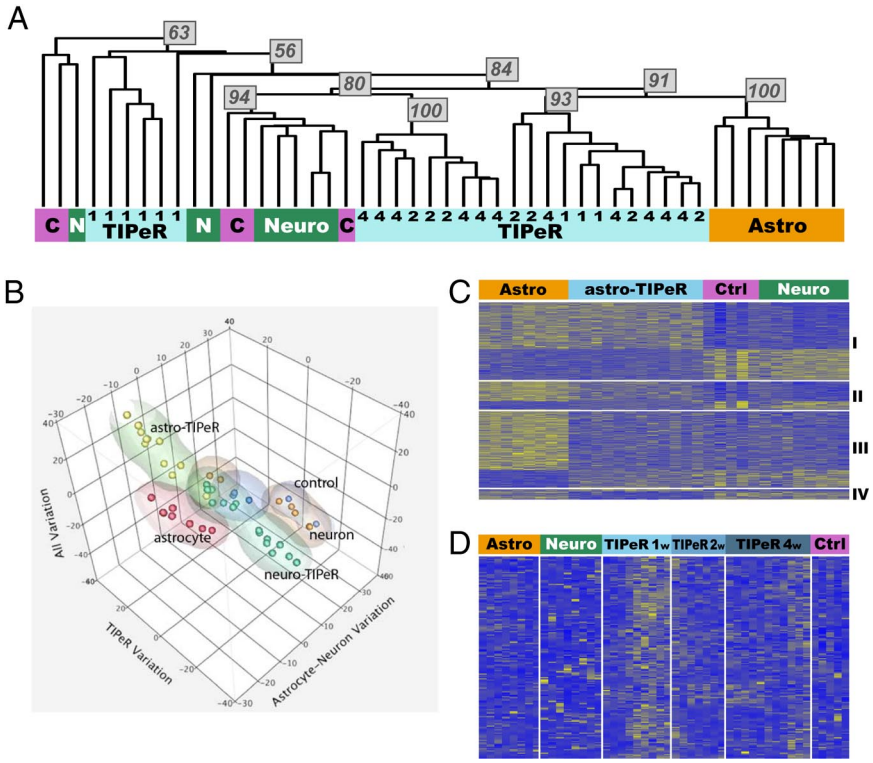

Fig. 3. Global gene expression patterns of TIPeR cells. (*A*) Unweighted Pair Group Method with Arithmetic (UPGMA) clustering of the cell conditions on 3,104 informative genes, with major branches labeled with bootstrap support, indicating confidence in each cluster. Leaves are colored according to cell type: (*green*) neurons, (*purple*) N-TIPeR-N controls, (*blue*) TIPeRed cells, (*orange*) astrocytes. (*B*) We visualized the 3,104-dimensional standard-gene space by reducing the high-dimensional coordinates to 3 dimensions of biological interest: the first axis represents genes most variable for astrocyte vs. neurons, the second axis represents genes most variable between the TIPeR cells (i.e., representing TIPeR treatment variability), and the third axis representing overall variability of all cells [(*red*) astrocytes, (*orange*) neurons, (*blue*) control. (*yellow*) astro-TIPeR (i.e., the TIPeR cells clustering closest to the astrocytes as shown in the dendrogram in *A*), (*green*) neuro-TIPeR]. The transparent "cloud" around the points shows nonparametric density contours. (see *Materials and Methods*). (*C*) Heatmap showing intensity of 512 distinguishing probes (see *Materials and Methods*) across astrocytes (Astro), astro-TIPeRs (astro-TIPeR), N-TIPeR-N controls (Ctrl), and neurons (Neuro). Probes are separated by white lines into 4 groups according to the intensities of the astro-TIPeR cells compared to the intensities of the neurons and the astrocytes: (I) astro-TIPeR expression is similar to astrocytes but not neurons (201 probes); (II) astro-TIPeR expression is intermediate between astrocytes and neurons (77 probes); (III) astro-TIPeR expression is similar to neurons but not astrocytes (202 probes); (IV) astro-TIPeR expression is dissimilar to both neurons and astrocytes (32 probes). Each lane is the data from an individual cell. (*D*) Heatmap of 171 probes that are significantly quiescent in both astrocytes (Astro) and neurons (Neuro); followed by TIPeR cells 1 week (TIPeR 1w), 2 weeks (TIPeR 2w), and 4 weeks (TIPeR 4w) after phototransfection, and for control cells (Ctrl). These genes show significant de novo up-regulation in TIPeR cells, especially in 1-week cells. No de novo up-regulation is seen in control cells. Each lane is the data from an individual cell.

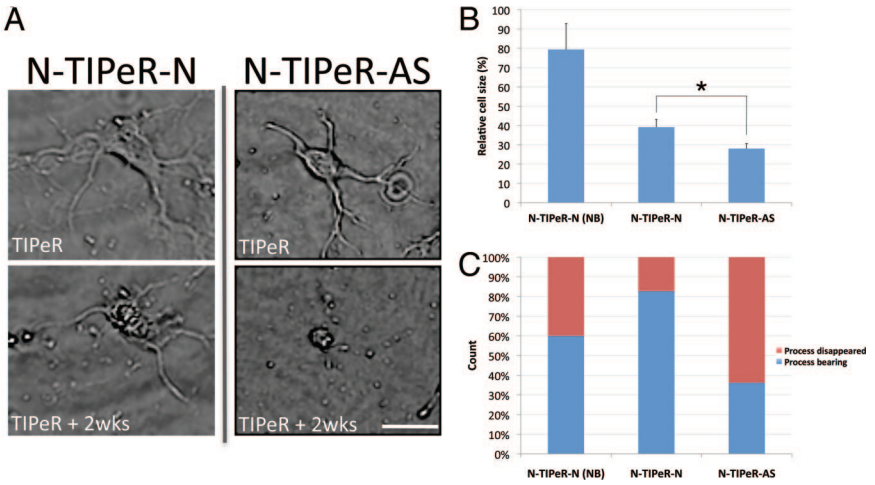

Fig. 4. Morphological analysis of TIPeR cells. (*A*) DIC images of representative N-TIPeR-N cell (*Left*) and N-TIPeR-AS cell (*Right*) demonstrate that the N-TIPeR-AS cell shows significant decreased overall size, including retraction of all its processes while the N-TIPeR-N cell only shows a slightly decreased cell size with most of its processes intact. (Scale bar, 20 μm.) (*B*) N-TIPeR-AS cells show significant decrease in relative size when comparing to that of N-TIPeR-N cultured in the neuronal media or in the astrocyte media. The *y*-axis is the percentage of change in overall cell size when comparing that of post-TIPeR to the initial cell size. Error bars represent the value of the SEM. ($*P < 0.05$) (*C*) Process retraction occurs for N-TIPeR-AS cells with 65% of N-TIPeR-AS cells showing retraction of their processes while only 40% of N-TIPeR-N cells cultured in the astrocyte medium and 20% of N-TIPeR-N cells cultured in the neuronal medium (NB) retracted their processes.

(see Fig. 2*A*) shows that the *GFAP* gene has been de novo transactivated and that endogenous GFAP mRNA is made as also seen by the changes in global gene expression (see Fig. 3*C*). To further confirm transactivation of genes by donor RNA, we delineated genes whose expression level was significantly low in both neurons and astrocytes. If any of these genes show increased expression in N-TIPeR-AS cells distinct from control TIPeR cells, it would indicate de novo up-regulation. Out of the 3,104 informative genes (see *Materials and Methods*), we found 171 genes that were quiescent in both neurons and astrocytes ($P < 0.05$) (see *SI Materials and Methods*). For each of these genes, we tested for significant up-regulation ($P < 0.05$) in 1-week ($n = 9$), 2-week ($n = 7$), and 4-week ($n = 11$) N-TIPeR-AS cells, and in N-TIPeR-N control cells ($n = 5$), respectively, against the astrocytes and neurons ($n = 16$). We found significant up-regulation of 49 (1 week), 17 (2 week), and 24 (4 week) genes in N-TIPeR-AS cells and none in N-TIPeR-N control cells (see Fig. 3*D*). The 1-week postphototransfection N-TIPeR-AS cells show the greatest number of significantly up-regulated genes. Because we selected for genes that are quiescent in the original astroctye transcriptome, we expected the expression of these genes to decrease in the N-TIPeR-AS cell with maturation of the reprogramming process: this prediction was confirmed in 2-week and 4-week N-TIPeR-AS cells (see Fig. 3*D*). Interestingly, GO annotation suggests that the de novo up-regulated genes are enriched for chromosome- and DNA metabolism-related processes (Tables S2 and S3), indicating a chromosomal remodeling response to donor RNA. Our set of 3,104 informative genes already excludes genes involved in phototransfection-specific systemic effects, and we found no de novo up-regulation in N-TIPeR-N controls. These results are consistent with transient up-regulation of a subset of genes soon after the introduction of new RNA, putatively induced by transfactors translated from the donor RNA.

Morphological Analysis of TIPeRed Cells. The morphology of the N-TIPeR-AS cells was assessed using MetaMorph software (Molecular Devices) and showed a substantial reduction in cellular size (72% reduction from initial cell size, $n = 27$), including both soma and retained processes (Fig. 4*B*). Control N-TIPeR-N cells showed a smaller reduction in overall size when cultured in neuronal medium (21%, $n = 15$) than when cultured in astrocyte medium (61%, $n = 29$). In addition, there was a significant retraction of processes in the N-TIPeR-AS cells that is not observed in N-TIPeR-N neurons grown under either culture conditions. Data shown in Fig. 4*C* reveal that over 60% of the N-TIPeR-AS cells retracted all processes, whereas only 12% and 37% of N-TIPeR-N control cells cultured in astrocyte medium and neuronal medium, respectively, show retracted process morphologies. Thus, the astrocyte transcriptome appears to have induced both a size reduction and a dramatic loss of the neuron-critical processes. The different morphological effects of the neuronal and astrocyte transcriptomes upon the same host-cell type (hippocampal neuron) highlight the transcriptome-specific effects. The N-TIPeR-AS cells show a morphology that is smaller than that of a prototypical astrocyte. The culture conditions likely contribute to the observed morphology as it is likely that replating after phototransfection would permit unconstrained membrane remodeling (11).

N-TIPeR-AS Cells Display Astrocyte-Like Physiological Responses. Cellular physiology results from the coordinate expression and function of multiple gene products. Given the microarray data (see Fig. 3) showing the development of an astrocyte-like expression profile in the N-TIPeR-AS cells, we wondered whether this global change in gene expression would result in an astrocyte-like physiology. Intracellular calcium plays an important role in physiological processes, and imaging of changes in intracellular calcium levels has been used to characterize unique neuronal and astrocytic physiologies (15, 16). Both neurons and astrocytes express glutamate receptors and show increased intracellular calcium when exposed to glutamate. Astrocytes, unlike neurons, do not show rapid calcium increases upon KCl application. In Fig. 5 we show that before TIPeR, 100% of the cells identified as neurons (25 out of 25 cells;

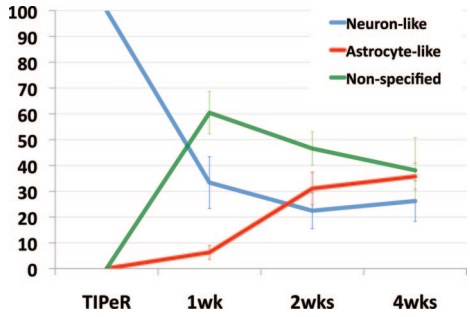

Fig. 5. N-TIPeR-AS cells display astrocyte-like physiological responses. The percentage of N-TIPeR-AS cells displaying astrocyte-like calcium fluctuation pattern [at least 5% increase in Fluo-4 intensity only upon glutamate (500 μM) but not KCl (50 mM) application] increased with time after the third phototransfection elongated (*blue line*). The percentage of N-TIPeR-AS cells still displaying neuron-like calcium fluctuation pattern (at least 5% increase in Fluo-4 a.m. intensity upon both glutamate and KCl application) decreased with time after the third phototransfection (*red line*). Nonspecified N-TIPeR-AS cells are the cells that show no detectable change upon glutamate application (*green line*). The *y*-axis represents the percentage of N-TIPeR-AS cells tested falling into these 3 groups at a given time point. Error bars are the SEM.

designated pre-N-TIPeR-AS) displayed neuronal activity [calcium increases in response to both glutamate (500 μM) and KCl (50 mM) application]. After TIPeR, the percentage of cells with neuronal responses decreased to 33% (16 out of 48 cells) by 1 week, 22% (13 out of 58) after 2 weeks, and 26% (11 out of 42) after 4 weeks. Cells displaying astrocyte-like activities (calcium increases only upon glutamate, but not KCl application) grew from 0% (0 out of 25 cells) before TIPeR to 6% (3 out of 48 cells) after 1 week, 31% (18 out of 58 cells) after 2 weeks, and 36% (15 out of 42 cells) after 4 weeks. At the initiation of the TIPeR process, all of the cells express host neuron-like physiological responses, and with time the number of N-TIPeR-AS cells showing neuron-like physiology decreases. As this decrease occurs, a population of cells that is physiologically undefinable as neurons or astrocytes becomes prominent at 1 week and then recedes as the number of physiologically astrocyte-like cells increases. This indeterminate physiology may represent the initial response of the neuronal hosts to TIPeR, which is also seen as Neuro-TIPeR cells in the microarray data (see Fig. 3 *A* and *C*). These data suggest that the astrocyte-like physiology of the N-TIPeR-AS cells increases as a function of time postphototransfection, in accord with the progression seen in the single-cell RT-PCR and single-cell expression-profiling data.

Discussion

The phenotype conversion of mature differentiated nondividing neurons upon phototransfection of the astrocyte transcriptome shows that mitosis is not necessary for stable long-term changes in the host-cell genome to occur. Furthermore, the cells were derived from low-density primary culture and position-tracked with microgrids, thereby precluding cell heterogeneity or fusion. Examples, such as the controversy with putative conversion of neural stem cells into hematopoetic cells emphasizes the need for careful cell-lineage discrimination (17). Here we achieve robust cell-lineage discrimination through individual cell tracking and single-cell assays. The efficiency of conversion was remarkably high and consistent over several criteria (RT-PCR 10 out of 26 = 38%; transcriptome 12 out of 27 = 44%; physiology 15 out of 42 = 36% at 4 weeks), each of which represents separate batches of TIPeR experiments. Thus, we conclude that the plasticity of the nondividing genome is much greater than previously envisioned. Our finding also suggests that the relative abundances of RNAs within a population themselves serve as important information for elaborating cellular phenotype. While reprogramming between other cell types remains to be explored, a critical aspect of transcriptomes as inducers of transdifferentiation is that they can be directly obtained from the donor cells and potentially be made with proper transcript ratios in a high-throughput manner, avoiding the need to search for the key transformation factors.

TIPeR-induced phenotype remodeling involves long-term changes in the host-cells' transcriptional pathways. As of yet it is unclear how other host-cell organelles, such as the mitochondria, are affected by the nuclear remodeling that occurs. Indeed, mitochondrial function is a dynamic process with protein trafficking between nucleus and the organelle that is regulated by cellular physiologies (18). Thus, mitochondria and other cellular organelles have the potential to be altered by TIPeR to create cell type-specific organelles. Such remodeling would have importance for manipulating various environmentally induced illnesses as well as other organelle-dependent processes, such as aging.

Despite common conventions, exact characterization of a cell type's phenotype is difficult. As reflected in Fig. 3*B*, there is a volumetric space of the range RNA expression (region of identity) that defines the neuronal or astrocytic phenotypes. These data highlight the need to use single-cell methodologies for analysis and understanding of cellular phenotype. The phenotype of cells correspond, not to a static molecular state but to a dynamic flux of molecular compositions that, as an aggregate, result in a recognizable suite of traits. A close analogy might be found in ecological communities. Distinct community assemblies, such as "conifer forest," "prairie," and so forth are recognized where each draws differentially from a common pool of possible organisms to form dynamic yet quasi-stable assemblies (19). An ecological community type is determined by self-organized regulatory control that is recognizable precisely because of its relative stability. Similarly, we suggest that the type of a cell and its cellular phenotype is determined not by the end product (e.g., proteins or RNA), but by the state of the control system: that is, the regulation state of its molecular physiology. A state of regulation is distinct from the molecular composition of the cell as much as "forest" and "grassland" are distinct from "pine" and "grass."

In Waddington's epigenetic landscape model, the process of cell development and differentiation was analogized as a marble rolling down from the apex of a hilltop (an embryonic stem cell) with multifurcating valleys and ridges (1). The iPS cells show that for at least some differentiation pathways, the original path is reversible, going back "up the hill" to the pluripotent state while our TIPeR data show that it is possible to move directly over the ridges that separate cellular phenotypes. However, our results show that the Waddington landscape metaphor, with its implied directionality, is not quite appropriate. As mentioned, a cell's state is defined not simply by DNA, proteins, RNAs, small molecules, and so forth, but by its self-organized regulatory state. During differentiation, a cell might start at one kind of quasi-stable state and evolve to other kinds of states, where it is the sequence of initial conditions that determine the seemingly irreversible directionality. Similarly, in ecology a classic concept is that of community succession, where one type of community was thought to displace another in sequence. But now this phenomenon is seen as a consequence of reversible ecological dynamics following natural dynamic flow (20). Thus, we propose that the appropriate metaphor for determination of a cell type is not a top-down flow of decisions but that of an "ecology of molecules" whose quasi-stable configurations form the harmonious and stable cell phenotypes, while the unstable intermediate configurations form the disharmonious, transient cell phenotypes. We note that the research problems of ecology mirror much of the problems related to cellular phenotypes (21).

The ecology metaphor can also be extended to the problem of switching between different cellular phenotypes. Restoration ecology aims to change ecological communities through interventions. Ideally, we would know the regulatory factors that determine each ecological community. However, even without such knowledge, we may still induce a switch-over from, for example, grasslands to forests, by introducing fast-growing trees and perhaps some inorganic factors. The key is that the community is not defined by a fixed set of driving instructions but by an interplay of self-organized dynamics. Thus, a change in part of the variables, for example the number of fast-growing trees, can form the right initial conditions to induce a switch-over. The transcriptome is not the regulatory system in of itself. But, the transcriptome in a particular state may represent the right set of initial conditions to induce regulatory switch-over. Our experiments suggest that such a procedure may be successful.

An important consequence for applications that arise from this framework is that the quasi-stable states are likely to be dynamic attractors, thus the perturbation for reprogramming need not be exact but merely "place" the cell somewhere within the attraction zone. This also suggests any transdifferentiation may have a myriad of possible recipes without a single master set of genes. Our astro-TIPeR cells should be viewed as astrocyte-like. One interpretation is that these cells are trapped in other quasistable states nearby astrocytes. Thus, we propose that mapping the harmonious transition pathway between different cell types through transcriptome manipulations may open the door to general cellular reprogramming recipes.

Materials and Methods

RNA Isolation, Amplification, and Array Analysis. Rat astrocytic transcriptome was extracted from the astrocyte culture using a TRIzol Reagent and MicroFast-Track 2.0 Kit. The host-hippocampal culture was prepared as previously described (22). After TIPeR, some coverslips were assessed using standard calcium imaging and immnucocytochemistry methods. The rest of the samples were assessed using standard single-cell harvesting and aRNA amplification methods, as previously described (23–25). For the final aRNA synthesis, the Ambion Illumina TotalPrep RNA Amp kit was used with an incubation time of 14 h. The aRNA obtained from individual TIPeRed cells was used for nested RT-PCR to detect the expression of GFAP and MAP2, and for Affymetrix Rat 230 2.0 analysis, where there was a volume of 40 μl, containing 2 μg of aRNA.

Phototransfection. RNA mixed with Lucifer Yellow was ejected over a neuron. The phototransfection was initiated when Lucifer Yellow fluorescence was saturated; the titanium-sapphire laser created 16 random transient poration sites with 5-ms intervals between each pulse by delivering laser pulses for 5 ms at a power of 35 mW. The second and third phototransfection were performed 48 h and 7 days later, as above but with lower laser power (30 mW). After phototransfection the cells were cultured in astrocyte medium supplemented with arachidonic acid and Dharmafect3 to bolster host-cell lipid composition during the TIPeR-induced remodeling of cellular phenotype (26, 27).

Immunocytochemistry. Cells were fixed using 4% paraformaldehyde and permeablized using 0.2% triton-X for 15 min at room temperature. Antibodies used for immunocytochemistry included GFAP (1:250) for 1 h at 37 °C, followed by incubation with goat anti-mouse secondary antibody conjugated with Alexa 546 (1:500), NeuN (1:50), followed by incubation with goat anti-mouse secondary antibody conjugated with Alexa 488 (1:500) or fibronectin (1:250), followed by incubation with goat anti-rabbit secondary antibody conjugated with Alexa 647 (1:500).

Calcium Imaging. Calcium imaging was performed with Fluo-4 on a confocal microscope. Intracellular calcium changes were imaged in 3-sec intervals. For analysis, regions of interest were selected based on reference DIC image of cells that were taken during the TIPeR procedure. Background-subtracted fluorescent signal intensity ($\Delta F/F$) was used to evaluate physiological responses.

Single Cell Nested RT-PCR. Primer sequences for GFAP are outer (5′-AGTGGCCACCAGTAACATGCAA-3′, 5′-TTGTCTTGCTCCAGCAGCCTAT-3′) and inner (5′-AGAAACCAGCCTGGACACCAAA-3′, 5′-TGGGAATTGGGCCTAG-CAAACA-3′), and for MAP2 are outer (5′-ATGGCCACCAAGACCTTGGAAA-3′, 5′-ACGGACTTTGTCATCGGTTCCT-3′) and inner (5′-TGGAGGGCAAACTAC-CCAAGTT-3′, 5′-ATCAGCAACAGGTGGCAAACCA-3′).

Computational Analysis of Single-Cell Transcriptome. ***Transcriptome quantification.*** For each single-cell microarray measurements, probes with pervasive low-quality measurements were removed (as reported by Affymetrix MAS 5.0) and expression intensities were corrected with the Robust Multichip Average algorithm (28), quantile normalized, and summarized using an upper-decile statistic [Bioconductor (16), affyPLM (29)]. Phototransfection effect was controlled by removing genes that differentiate the N-TIPeR-N cells from the neurons (Welch's *t* test). Our quality control left 3,104 most informative genes for further analysis.

Bootstrap cluster analysis. We clustered the cells based on their expression with the Euclidean and standard UPGMA clustering method. To assess the robustness of the clusters, we generated a set of 1,000 bootstrap-resampled 3,104 informative genes, recomputed an UPGMA cluster tree for each, and then computed a consensus tree using PHYLIP. For each cluster in the consensus tree, we counted the frequency of each cluster in the 1,000 resampled data sets.

Delineating gene sets of biological interest. Within our informative set of 3,104 genes, we identified genes of interest as the top 10% difference (Welch's *t* test) and at least a 2-fold differential that contrast the following biological conditions: astrocyte vs. neurons (630 genes), astrocyte vs. astro-TIPeR (136 genes), neurons vs. astro-TIPeR (43 genes), astro-TIPeR vs. neuro-TIPeR (560 genes). Using same criterion, we also generated a set of significantly similar gene groups as: astrocyte = astro-TIPeR (69 genes), neuron = astro-TIPeR (46 genes), astro-TIPeR = neuro-TIPeR (370 genes).

Visualizing transcriptome space. To generate each axis shown Fig. 3*B*, we used the gene sets from each biological contrast of interest and found the principal direction of variation for each gene set along with the principal direction of variation for all genes.

Transactivation of genes by donor astrocyte RNA. For each of the 3,104 informative genes, we computed Fisher's combined *P*-value for their expression rank in the 8 (neurons) + 8 (astrocyte) = 16 single-cell transcriptomes. The resulting *P*-values were multiple-test corrected for 3,104 genes using Bonferroni correction and cutoff at the 5% significance level, leaving 171 significantly low-expressed genes. For each of the contrasts discussed in the main text, we carried out pair-wise Welch's *t*-tests for increased expression for each of these cell types against the combined group of 16 astrocyte plus neurons.

See *SI Materials and Methods* for further discussion of the methods used.

ACKNOWLEDGMENTS. We thank Dr. Izabella Klein for suggesting the use of a single-stranded DNA carrier in the PCR reactions. This work was supported in part by Human Resources Fact Finder funds from the Commonwealth of Pennsylvania (J.Y.K.), National Institute of Health Grant T32-MH14654 (to C.K.W.), Department of Energy Fellowship, DE-FG02–97ER25308 (to M.T.L.), and the National Institute of Health Director's Pioneer Award Program, DP1-OD-04117 (to J.E.). The Keck Foundation provided important support for this project.

1. Waddington (1957) *The Strategy of the Genes: a Discussion of Some Aspects of Theoretical Biology* (George Allen & Unwin, London).
2. Gurdon JB, Elsdale TR, Fischberg M (1958) Sexually mature individuals of *Xenopus laevis* from the transplantation of single somatic nuclei. *Nature* 182(4627):64–65.
3. Takahashi K, Yamanaka S (2006) Induction of pluripotent stem cells from mouse embryonic and adult fibroblast cultures by defined factors. *Cell* 126(4):663–676.
4. Huangfu D, et al. (2008) Induction of pluripotent stem cells from primary human fibroblasts with only Oct4 and Sox2. *Nat Biotechnol* 26(11):1269–1275.
5. Kim JB, et al. (2008) Pluripotent stem cells induced from adult neural stem cells by reprogramming with two factors. *Nature* 454(7204):646–650.
6. Nakagawa M, et al. (2008) Generation of induced pluripotent stem cells without Myc from mouse and human fibroblasts. *Nat Biotechnol* 26(1):101–106.
7. Maherali N, et al. (2007) Directly reprogrammed fibroblasts show global epigenetic remodeling and widespread tissue contribution. *Cell Stem Cell* 1(1):55–70.
8. Okita K, Ichisaka T, Yamanaka S (2007) Generation of germline-competent induced pluripotent stem cells. *Nature* 448(7151):313–317.
9. Stadtfeld M, Nagaya M, Utikal J, Weir G, Hochedlinger K (2008) Induced pluripotent stem cells generated without viral integration. *Science* 322(5903):945–949.
10. Wernig M, et al. (2008) Neurons derived from reprogrammed fibroblasts functionally integrate into the fetal brain and improve symptoms of rats with Parkinson's disease. *Proc Natl Acad Sci USA* 105(15):5856–5861.
11. Hanna J, et al. (2007) Treatment of sickle cell anemia mouse model with iPS cells generated from autologous skin. *Science* 318(5858):1920–1923.
12. Barrett LE, et al. (2006) Region-directed phototransfection reveals the functional significance of a dendritically synthesized transcription factor. *Nat Methods* 3(6):455–460.
13. Anderson DJ, Gage FH, Weissman IL (2001) Can stem cells cross lineage boundaries? *Nat Med* 7(4):393–395.
14. Valles S, Pitrach J, Renau-Piqueras J, Guerri C (1997) Ethanol exposure affects glial fibrillary acidic protein gene expression and transcription during rat brain development. *J Neurochem* 69:2484–2493.
15. Rowe EW, Jeftinija DM, Jeftinija K, Jeftinija S (2005) Development of functional neurons from postnatal stem cells in vitro. *Stem Cells* 23(8):1044–1049.
16. Gentleman RC, et al. (2004) Bioconductor: open software development for computational biology and bioinformatics. *Genome Biol* 5(10):R80.
17. D'Amour KA, Gage FH (2002) Are somatic stem cells pluripotent or lineage-restricted? *Nat Med* 8(3):213–214 .
18. Zhang J, et al. (2008) Altered proteome biology of cardiac mitochondria under stress conditions. *J Proteome Res* 7(6):2204–2214.
19. Loreau M, et al. (2001) Biodiversity and ecosystem functioning: current knowledge and future challenges. *Science* 294(5543):804–808.
20. McCook LJ (1994) Understanding ecological community succession: causal models and theories, a review. *Plant Ecology* 110(2):115–147.
21. Thomson JN et al. (2001) Frontiers of Ecology. *BioScience* 51(1):15–24.
22. Cummings DD, Wilcox KS, Dichter MA (1996) Calcium-dependent paired-pulse facilitation of miniature EPSC frequency accompanies depression of EPSCs at hippocampal synapses in culture. *J Neurosci* 16:5312.
23. Van Gelder RN, et al. (1990) Amplified RNA synthesized from limited quantities of heterogeneous cDNA. *Proc Natl Acad Sci USA* 87:1663.
24. Eberwine J, Crino P (2001) Analysis of mRNA populations from single live and fixed cells of the central nervous system. *Curr Prot Neurosci* Chapter 5, Unit 5 3.
25. Eberwin J (2001) Single cell molecular biology. *Nat Neurosci* 4 Suppl, 1155–1156.
26. Fukaya T, et al. (2007) Arachidonic acid preserves hippocampal neuron membrane fluidity in senescent rats. *Neurobiol Aging* 28(8):1179–1186.
27. Neufeld EJ, Majerus PW, Krueger CM, Saffitz JE (1985) Uptake and subcellular distribution of [3H]arachidonic acid in murine fibrosarcoma cells measured by electron microscope autoradiography. *J Cell Biol* 101(2):573–581.
28. Bolstad BM, Irizarry RA, Astrand M, Speed TP (2003) A comparison of normalization methods for high density oligonucleotide array data based on variance and bias. *Bioinformatics* 19:185–193.
29. Bolsdtad B (2005) affyPLM: Methods for fitting Probe-lvel models. In R package (Bioconductor, www.bioconductor.org).